Measurement of the Low-Energy End of the μ^+ Decay Spectrum*†

STEPHEN E. DERENZO‡
The Department of Physics and The Enrico Fermi Institute, The University of Chicago, Chicago, Illinois 60637
(Received 12 November 1968)

The μ^+ decay spectrum has been measured below 6.8 MeV/c using a hydrogen bubble chamber. The chamber was calibrated as an electron spectrometer using the 0.9- and the 1.4-MeV/c internal conversion lines from a Bi^{207} source. When the measured distribution was fitted to the Michel spectrum, the low-energy parameter η was found to be -0.13 ± 0.20, with ρ constrained to be $\frac{3}{4}$. A two-parameter fit incorporating published data from spark-chamber measurements of the upper half of the spectrum gave the values $\eta=-0.12\pm0.21$ and $\rho=0.752\pm0.003$.

I. INTRODUCTION

THE decay of the muon is of fundamental significance in the study of weak interactions, since it is at present the only experimentally accessible weak process free from the complications of strong interactions. Assuming a local (derivative-free) and lepton-conserving interaction, the most general Hamiltonian is[1]

$$H=\sum_{i=1}^{5}(\bar{e}\Gamma_i\mu)[\bar{\nu}\Gamma_i(C_i+C_i'\gamma_5)\nu], \quad (1)$$

where the index i runs through scalar, vector, tensor, axial vector, and pseudoscalar couplings. This ordering of the field operators is the one most commonly found in the literature, and can be related uniquely to any other ordering by a Fierz-Michel transformation.[2]

The spectrum,[3–7] asymmetry,[7,8] and helicity[9,10] of the decay electrons have been studied by many "high-statistics" experiments that have yielded values for four parameters, namely, ρ, ξ, δ, and h. The definitions of these parameters in terms of the coupling constants are given in Ref. 1 and in the Appendix.

This paper describes in detail[11] the first precise study of low-momentum positrons (below 6.8 MeV/c) from μ^+ decay. This region of the spectrum is sensitive to the parameter η (defined in the Appendix), and its study provides new information about the fundamental coupling constants. Although there are too few experimentally observable parameters to uniquely determine all ten (possibly complex) coupling constants, it is nevertheless possible to place useful limits on some of them. A summary of the coupling constants and their possible values is given in the Appendix.

A. Michel Spectrum

Assuming the Hamiltonian of Eq. (1), Michel has shown[12,13] that the isotropic muon decay spectrum is completely determined, given two bilinear combinations of the coupling constants ρ and η. Correct to all orders in m_e/m_μ, the most convenient form of the Michel spectrum is

$$N(y;\rho,\eta)=(y^2-y_0^2)^{1/2}[6y(1-y)+\tfrac{4}{3}\rho(4y^2-3y-y_0^2)+6y_0\eta(1-y)], \quad (2)$$

where $y=E/E_{\max}$, E=total positron energy, $E_{\max}=52.83$ MeV, and $y_0=m_e/E_{\max}$.

B. Electromagnetic Modifications

The electromagnetic corrections to Eq. (2) have been calculated by Kinoshita and Sirlin[1,14] and by Berman[15] assuming a local V−A theory. Scalar, tensor, and pseudoscalar couplings were excluded since they gave results depending upon an arbitrary cutoff, and the electron was assumed to be massless (which has the effect of setting η to zero). Grotch[16] performed the same calculation in the more general $V+\epsilon A$ theory, keeping terms linear in the electron mass. His calculation is applicable even to experiments measuring the low end

* Work supported by the National Science Foundation (Grant Nos. GP-6135, GP-9093, and GP-6464) and by the Office of Naval Research [Contract No. Nonr-2121(25)].
† A thesis submitted to the Department of Physics, The University of Chicago, in partial fulfillment of the requirements for the Ph.D. degree.
‡ Fellow, Associated Midwest Universities Argonne National Laboratory 1965–1966 and Shell Foundation 1967–1968. Present address: Lawrence Radiation Laboratory, Berkeley, California.
[1] T. Kinoshita and A. Sirlin, Phys. Rev. **107**, 593 (1957).
[2] J. D. Jackson, Brandeis Lecture, 1962 (unpublished); D. B. Fierz, Z. Physik **104**, 553 (1937).
[3] W. Dudziak, R. Sagane, and J. Vedder, Phys. Rev. **114**, 336 (1959).
[4] R. J. Plano, Phys. Rev. **119**, 1400 (1960).
[5] M. Bardon, P. Norton, J. Peoples, A. M. Sachs, and J. Lee-Franzini, Phys. Rev. Letters **14**, 449 (1965); J. Peoples, Columbia University Report No. NEVIS-147, 1966 (unpublished).
[6] B. A. Sherwood, Phys. Rev. **156**, 1475 (1967).
[7] D. Fryberger, Phys. Rev. **166**, 1379 (1968).
[8] I. I. Gurevich, L. A. Makariyna, B. A. Nikol'sky, B. V. Sokolov, L. V. Surkova, S. KH. Khakimov, V. D. Shestakov, YU. P. Dobretsov, and V. V. Akhmanov, Phys. Letters **11**, 185 (1964).
[9] P. C. Macq, K. M. Crowe, and R. P. Haddock, Phys. Rev. **112**, 2061 (1958); G. Culligan, S. G. F. Frank, and J. R. Holt, Proc. Phys. Soc. (London) **73**, 169 (1959).
[10] D. M. Schwartz, Phys. Rev. **162**, 1306 (1967).
[11] Preliminary results of this experiment have been reported [S. E. Derenzo and R. H. Hildebrand, Phys. Rev. Letters **20**, 614 (1968); S. E. Derenzo, R. H. Hildebrand, and C. Vossler Phys. Letters **28B**, 401 (1969)].
[12] L. Michel, Proc. Phys. Soc. (London) **A63**, 514 (1950).
[13] C. Bouchiat and L. Michel, Phys. Rev. **106**, 170 (1957).
[14] T. Kinoshita and A. Sirlin, Phys. Rev. **113**, 1652 (1959).
[15] S. M. Berman, Phys. Rev. **112**, 267 (1958).
[16] H. Grotch, Phys. Rev. **168**, 1872 (1968).

of the spectrum, where the electron is not highly relativistic. Florescu and Kamei[17] have computed the electromagnetic corrections within the framework of a general (S,V,T,A,P) theory, and their results depend upon a cutoff. The electromagnetic corrections that arise when the weak process is mediated by a vector boson, have been calculated by Bailin[18] assuming a V−A interaction. In Sec. VI C, this theory is applied to our result in order to place a lower limit on the vector-boson mass.

Figure 1 shows the fractional change in the spectrum, which occurs when η is increased from 0 to $\frac{1}{2}$, and Fig. 2 shows the ratio of the electromagnetic correction of Grotch to that change. It is seen that throughout the lower half of the spectrum, the radiative corrections are at least three times larger than the change that occurs when η is varied by $\frac{1}{2}$.

II. GENERAL DESCRIPTION OF THE EXPERIMENT

The 10-liter University of Chicago hydrogen bubble chamber was exposed to a beam of stopping π^+ and μ^+ from the Chicago synchrocyclotron. Two exposures were taken, using magnetic fields of 20.85 and 14.13 kG. A total of 424 000 frames were scanned, containing 2 070 000 μ^+ decays.

The decays were scanned in two distinct samples. Sample 1 represented the over-all decay spectrum as seen in every hundredth frame, and sample 2, taken from all other frames, consisted of events with sufficiently large radius of curvature to ensure that all events with momentum less than 7.1 MeV/c were included. Section II A describes in detail how this was done.

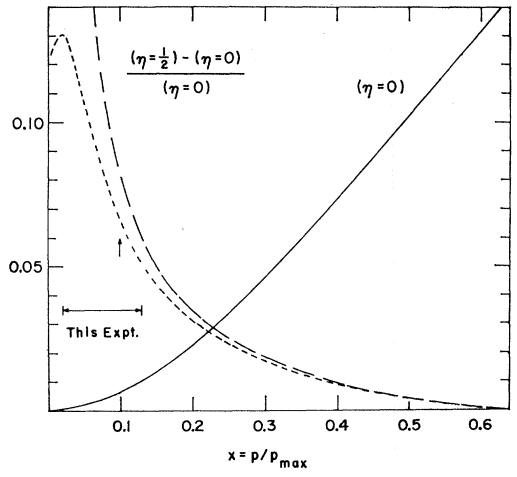

FIG. 1. Sensitivity of the decay spectrum to η. Solid line shows μ^+ decay spectrum for $\eta=0$. Long dashed line shows fractional change in spectrum before radiative corrections when η is varied from 0 to $\frac{1}{2}$. Short dashed line shows same change after radiative corrections. Arrow shows mean momentum for this experiment.

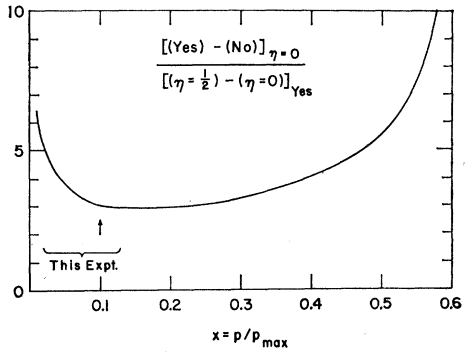

FIG. 2. Effect of the radiative correction. Curve shows ratio of change in spectrum due to radiative corrections to change which occurs when η is varied from 0 to $\frac{1}{2}$. Arrow shows mean momentum for this experiment.

The selected events were then measured and analyzed with the Three-View Geometry Reconstruction Program (TVGP), as described in Sec. II B.

The momentum measurements were calibrated by the 0.9- and 1.4-MeV/c internal-conversion-electron lines from a Bi^{207} source coated on Mylar (Du Pont registered trade mark) strips which were stretched across the chamber. These electrons appeared in the same pictures as the μ^+-decay positrons (see Fig. 3) and

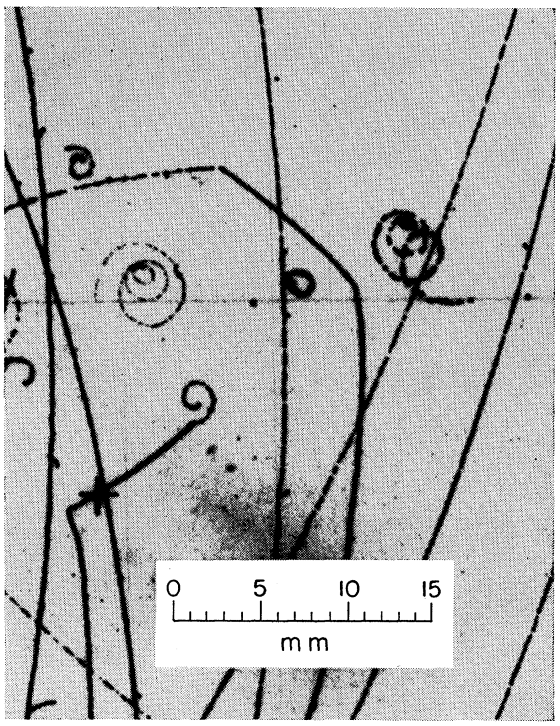

FIG. 3. Sample events. Picture shows two 1.4-MeV/c internal-conversion electrons emerging from the Mylar strip (faint horizontal line), and two $\pi^+-\mu^+-e^+$ decay chains. One of the positrons has a momentum of 0.7 MeV/c.

[17] Viorica Florescu and Osamu Kamei (to be published).
[18] D. Bailin, Phys. Rev. **135**, B166 (1964).

were subject to the same measurement procedures. This calibration is described in an earlier publication[19] and is summarized in Sec. III.

The corrections and errors including scanning inefficiency, measuring inefficiency, and the detailed shape of the resolution function are discussed in Sec. IV.

A. Scanning Requirements

The events of sample 1 were chosen on the basis of the following criteria: (i) A counterclockwise lightly ionizing track (e^+) must emerge from the end of the stopping μ^+ track; (ii) The positron track must begin within a defined scanning region. Sample-2 events were required to satisfy two additional conditions: (iii) The decay positron must turn through more than 90° as seen in view 1. (iv) At all points of its track in all three views the decay positron must have more curvature than a 7.1-MeV/c (zero-dip) positron. This limiting curvature was tested on the scanning tables by means of a circle of 2.50-cm radius during the 20.85-kG scanning and a circle of 3.75-cm radius during the 14.13-kG scanning. The Recordak scanning machines projected the film 2.2 times life size. It was shown by the construction of artificial tracks of various dip angles, that this test could never reject an electron whose momentum was less than 7.1 MeV/c. Examples of two conversion electrons, a sample-1 event and a sample-2 event, are shown in Fig. 3.

B. Measuring Procedure

The film was measured on the Chicago image-plane digitizing machines. Six to nine points, spaced about equally, were digitized on each track. The tracks were reconstructed using the TVGP developed by the Alvarez group.[20] The program was modified in three aspects to adapt it to our problem

(i) The general mass-independent range-momentum table was replaced with a table computed specifically for electrons.[21] (ii) TVGP was modified so that the program would accept the noncircular spirals typical of low-energy tracks turning through large angles. (iii) Instead of considering a track to start at the most downstream measured point in the "master" view, we used an average of the first measured points in all views.[22] This correction eliminated a tendency to overestimate the track length and had an average value of 0.01 cm or 0.003 MeV/c.

In order to determine the momentum of the highest possible fraction of events, it was necessary to measure a track piecewise if the positron suffered a Coulomb interaction with a proton (producing a kink) or an electron (producing a δ ray) shortly after decay.

III. CALIBRATION

The random and systematic errors of the spectrometer have been determined by applying the entire scanning, measuring, and track-reconstruction procedure to three momentum standards: the 0.875- and 1.414-MeV/c internal conversion electrons emitted by a Bi^{207} source, the μ^+ decay spectrum in the region of the cutoff at 52.83 MeV/c, and electron pairs from the reaction

$$\pi^- + p \rightarrow n + e^+ + e^-$$

(pair momentum 129.6 MeV/c). This reaction was studied by Kobrak[23] using the same bubble chamber. The main features of the calibration technique have been reported previously,[19] but significantly improved precision has now been achieved by better control of operating conditions, improved statistics, and more refined analysis procedures.

A. Conversion Electrons

The isotope Bi^{207} was introduced into the chamber in such a way that the conversion electrons were seen in the same pictures as the positrons from μ^+ decay. The isotope chosen Bi^{207} goes to excited states of Pb^{207} by K capture, and the Pb^{207} emits electrons by internal conversion. This source appears to be the best available for well-spaced accurately determined lines free of any charged-particle background. The half-life (28 yr) is convenient.

The principal transitions of Pb^{207} and the energies and relative intensities of the corresponding conversion-electron lines are shown in Table I. Since the centers of the observed peaks for the two principal transitions can be determined with errors that are small compared to the separation of the K, L, and M lines of each transition, it is essential to know the relative intensities, as

TABLE I. Conversion electrons from a Bi^{207} source.

Nuclear transition energy[a] (MeV)	Conversion electron	Electron momentum[b] (MeV/c)	Relative intensity[c]
0.56962	K	0.8510	1.7
	$L+M$	0.9375	0.63
1.06344	K	1.3958	8.2
	$L+M$	1.4752	2.58
1.76971	$K+L+M$	2.15	0.03

[a] Reference 26.
[b] Based on binding energies of Ref. 32. Figures for L electrons are averages of L_I, L_{II}, and L_{III} weighted by intensity ratios of Ref. 26. Figures for M electrons are averages of M_I, M_{II}, and M_{III} (M_{IV} and M_V negligible) weighted by conversion coefficients of Ref. 28 corrected for screening as in Ref. 27.
[c] K and L intensities from Ref. 25. M intensities from Refs. 27 and 28. $L+M$ intensity figures are for L_{I-III} and M_{I-III} combined (M_{IV} and M_V negligible). See Table III for further information on intensities.

[19] S. E. Derenzo and R. H. Hildebrand, Nucl. Instr. Methods **58**, 13 (1968).
[20] F. T. Solmitz, A. D. Johnson, and T. B. Day, Alvarez Group Programming Note P-117 (unpublished).
[21] M. J. Berger and S. M. Seltzer, NASA Report No. SP-3012, 1964 (unpublished).
[22] J. Hippard and P. Katz, listing of Argonne National Laboratory version of TVGP.
[23] H. Kobrak, Nuovo Cimento **20**, 1115 (1961).

well as the energies, of these lines. In preparing Table I we have used the experimental K/L intensity ratios and the transition energies reported by Alburger,[24] Alburger and Sunyar,[25] and Brady, Peek, and Warner.[26] For the K/M ratios we have applied the empirical screening corrections of Chu and Perlman[27] to the theoretical conversion coefficients of Rose[28] assuming that the 1.06–0.57 cascade is an $M4$–$E2$ cascade.[24–26,29–31] We have used the electron binding energies tabulated by Siegbahn.[32]

The Bi isotope, in the form of $Bi(NO_3)_3$, was dissolved in a solution of lucite in ethylene dichloride and this mixture was painted with a brush onto two 1-mil (0.025 mm)×1-mm type-S Mylar polyester strips leaving a layer 5 ± 2 μ thick. The concentration was such as to give nine conversion electrons per frame in the bubble-chamber pictures.

The two (parallel) strips were stretched across the chamber in the median plane at a separation of 3 cm (each passing 1.5 cm from the center). They were turned so that the cameras viewed them edgewise in order to minimize interference with the field of view. Figure 3 shows two 1.4 MeV/c conversion electrons emerging from one of the strips. The optical resolution indicated in this figure was achieved with careful design and adjustment of the optical system but without any novel techniques.

The energy loss of a conversion electron passing straight through 1-mil Mylar ($\sim$3.5 mg/cm^2) is 15 keV.[33] Since the source was deposited on only one side of each strip, we were able to correct the energy of the emerging electrons for losses in the Mylar and lucite. The average error in this correction is not larger than 3 KeV.

In order to find a complete description of our momentum resolution, various functions have been fit to the experimental data.

For an electron line of momentum p', the observed distribution is well represented by the function

$$f(p)=(p/p')^a/[|p-p'|^b+(\tfrac{1}{2}p'\Gamma)^b], \qquad (3)$$

where a, b, and Γ are parameters chosen to give the best fit. This function has the property that for typical values of a, b, and Γ, the full width at half-maximum (FWHM) is equal to Γ to an accuracy better than 0.5% (see Table III of Ref. 18). When the "skewing factor" a is positive, then Eq. (3) is zero at $p=0$. The factor b governs the size of the tails of the distribution.

An acceptable fit was made to the conversion-electron spectrum (Fig. 4) throughout the 0–3 MeV/c interval by the following sum:

$$F(p)=\sum_{i=1}^{5} A_i\frac{(p/p_i)^a}{|p-p_i|^b+(\tfrac{1}{2}p_i\Gamma_i)^b}, \qquad (4)$$

which is carried out over the five lines of Table I, each having position p_i, weight A_i, and FWHM Γ_i. The L and M components are sufficiently close together so that they may be represented by a single line shape. The fitting was done by varying six parameters: R, Δ, Γ_1, Γ_3, a, and b. The quantity R was defined as the ratio $(A_3+A_4)/(A_1+A_2)$, while the ratios A_1/A_2 and A_3/A_4 were taken from Table I. The line positions p_i were obtained by multiplying the values of Table I by the common factor $(1+\Delta)$ (See Table II, footnote b). For each principal transition, the FWHM was assumed to be equal for K, L, and M lines (i.e., $\Gamma_1=\Gamma_2$ and $\Gamma_3=\Gamma_4$). The 2.15-MeV/c transition, which makes an almost negligible contribution to the upper tail of the 1.4-MeV/c peak, was assumed to have the parameters $A_5=0.3\%$ of all conversion electrons and $\Gamma_5=\Gamma_3$. The results are shown in Table II.

B. Muon-Decay Spectrum at 53 MeV/c

The width Γ and systematic momentum error were determined at 53 MeV/c by comparing our sample-1 data with those of a recent precise counter measurement by Peoples.[5] A resolution function of the form given by Eq. (3) (where the shape parameters a and b were taken from Fig. 5) was folded into Peoples' histogram and fit to our data in the region from 47 to 63 MeV/c. Peoples' external bremsstrahlung corrections are comparable to ours (the systematic momentum error introduced by assuming them to be equal is less than 0.2%), and his resolution width $\frac{1}{3}$% influenced the estimate of our

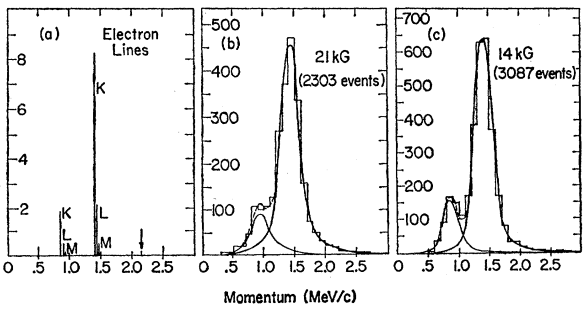

FIG. 4. Conversion-electron spectra. (a) Electron lines (see Table I). Arrow indicates mean momentum of electrons from the 1.7-MeV transition. (b,c) Histograms show events per 0.1 MeV/c in conversion-electron spectra. Solid curves are individual peaks and dashed curves are total spectra as obtained by fitting Eq. (4) to histograms.

[24] D. E. Alburger, Phys. Rev. **92**, 1257 (1953).
[25] D. E. Alburger and A. W. Sunyar, Phys. Rev. **99**, 695 (1955).
[26] F. P. Brady, N. F. Peek, and R. A. Warner, Nucl. Phys. **66**, 365 (1965).
[27] Y. Y. Chu and M. L. Perlman, Phys. Rev. **135**, B319 (1964).
[28] M. E. Rose, *Internal Conversion Coefficients* (North-Holland Publishing Co., Amsterdam, 1958).
[29] M. Goldhaber and A. W. Sunyar, Phys. Rev. **83**, 906 (1951).
[30] A. H. Wapstra, Arkiv Fysik **7**, 279 (1954).
[31] F. M. McGowan and E. C. Campbell, Phys. Rev. **92**, 523 (1953).
[32] *Alpha-, Beta-, and Gamma-ray Spectroscopt*, edited by Kai Siegbahn (North-Holland Publishing Co., Amsterdam, 1965).
[33] It is an adequate approximation to assume that the energy loss per unit thickness is the same for all electrons from the source (i.e., for the energy range of Table I).

TABLE II. Momentum errors.[a]

Magnetic field (kG)	Electron source	Momentum (MeV/c)	Systematic error[b] (%)	Observed FWHM (%)	FWHM from Eq. (7) (%)
14.1	Bi^{207}	0.9	-1.5 ± 0.5	32 ±3	34.0
14.1	Bi^{207}	1.4		24 ±1.5	25.1
14.1	μ^+ decay	52[c]	-1.4 ± 0.8	18 $+2$	17.2
20.9	Bi^{207}	0.9	-0.5 ± 0.7	38 ±5	34.2
20.9	Bi^{207}	1.4		24 ±2	24.1
20.9	μ^+ decay	52[c]	-0.6 ± 1.0	8.4 ± 1.0	8.4
24.7	$\pi^-+p\rightarrow n+e^++e^-$	65[d]	$+0.02$	8.9 ± 1.5	9.2

[a] All figures are for tracks with dip angles λ, such that $|\sin\lambda|\leqslant0.7$.
[b] The systematic error Δ is the difference in momentum between the measured and the "true" spectrum expressed as a fraction of the true momentum; i.e., $\Delta=[p(\text{measured})-p(\text{true})]/p(\text{true})$, where $p(\text{measured})=p_i$ of Eq. (3) adjusted for best fit.
[c] High-energy cutoff (see Sec. III B).
[d] Mean energy of electrons (see Sec. III C).

widths by less than 0.015%. The results for the 14- and 21-kG runs are given in Table II.

C. Internal Pairs from π^- Capture by Protons

Using the same bubble chamber, Kobrak[23] has studied 2141 electron pairs from the reaction $\pi^-+p\rightarrow n+e^++e^-$. The mean value of the experimental distribution is 129.8 MeV, which is in excellent agreement with the figure 129.55 MeV calculated with accepted values of the particle masses. The FWHM for this peak is 8.3 MeV/c or 6.3%. From this we infer that a distribution for single tracks of energy $129.55/2\simeq65$ MeV would have a FWHM $\Gamma=8.9\%$, which is in good agreement with the value $\Gamma=9.2\%$ obtained by fitting the data of Table II as described in Sec. III D.

D. Results of the Calibration

The shape of the resolution function was found to be adequately described by Eq. (3) at 0.9 and 1.4 MeV/c (see Fig. 4) and at 53 MeV/c (see Fig. 4 of Ref. 19). The shape parameters a and b and their uncertainty were found by fitting the Bi^{207} data to Eq. (4) and by plotting the χ^2 as shown in Fig. 5. The best-fit values for each run are indicated by triangles, and the one-standard-deviation contours are shown by ellipses. The spectrometer resolution was improved for the 14-kG run by better control of operating conditions. At this field we find that the distribution has smaller tails (see Fig. 4) and consequently a larger fitted value for b (see Fig. 5). The upper end of the μ^+ decay spectrum could not yield additional information about a and b since the parameters a, b, and Γ are too highly coupled.

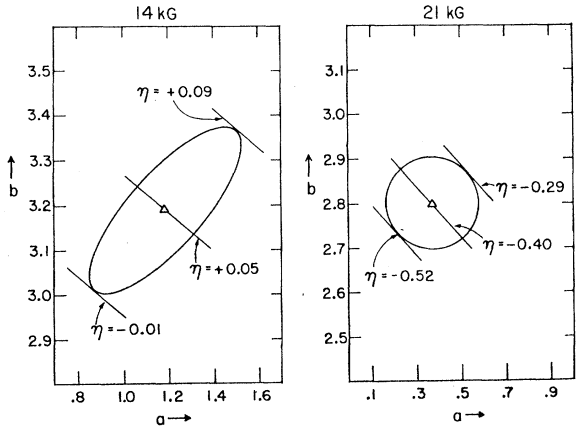

FIG. 5. η versus the shape parameters a and b. Ellipses show one standard deviation contours in a and b from fits to 14- and 21-kG Bi^{207} data. Triangles show best-fit values. The lines show values of a and b that result in the same fitted values for η.

From the agreement between the observed value of R and the accepted value (see Table III), it is concluded that proper corrections have been made for momentum-dependent effects. Unfortunately β-ray spectroscopists have not reported very precise values for R and our value at 14 kG given in Table III may be the best measurement of this ratio.

From the difference between the fitted and accepted peak locations (see Table II), we conclude that the parameter p' in Eq. (3) gives a value $0.5\pm0.7\%$ below the true line position for the 21-kG experiment and a value $1.5\pm0.6\%$ below the true line position for the 14-kG experiment.

In order to compare the observed μ^+ decay spectrum with the theoretical distributions, it was necessary to derive an expression for the FWHM as a function of momentum, as the calibration points of Table II do not directly indicate the resolution width appropriate for momenta between 1.4 and 53 MeV/c.

To determine the momentum error in measuring positron tracks, we used the analysis of Gluckstern.[34] The mean-square error in momentum (expressed as a fraction) is given by the expression

$$(\sigma_p/p)^2=[p\cos\lambda/(0.3B)]^2\sigma_c^2+(\tan\lambda\cot\theta_S)^2\sigma_\theta^2, \quad (5)$$

where p is the momentum in MeV/c, λ is the dip angle measured from the plane perpendicular to the magnetic-field direction, B is the magnetic field in kG, and θ_S is the stereo angle of the camera system ($\cot\theta_S\approx$distance from cameras to center of chamber divided by distance between cameras). The mean-square error in curvature σ_c^2 and the mean-square error in azimuthal angle σ_θ^2

[34] R. L. Gluckstern, Nucl. Instr. Methods 24, 381 (1963).

TABLE III. Relative intensities of conversion-electron lines.

Experiment	Quantities measured					R[a]
Alburger[b]; Alburger and Sunyar[c]	Transition	K electrons per 100 decays		$K/L_{I+II+III}$		
	1 MeV	8.2		3.95±0.25[b]		4.6[d]
	½ MeV	1.7		3.40±0.40[c]		
	1.7 MeV	0.022				
Brady, Peek, and Warner[e]	Transition	K electrons per 100 decays	K/L_I	K/L_{II}	K/L_{III}	
	1 MeV	8.0 ±0.5	6.24	8.33	28.6	4.4[d]
	½ MeV	1.7	5.26	27.0	58.8	
	1.7 MeV	0.022±0.013				
This experiment		Magnetic field (kG)				
		14				4.6±0.3[f]
		21				5.2±0.7

[a] Ratio of the sums of the K, L_{I-III}, M_{I-V} electron intensities for the 1- and ½-MeV lines.
[b] See Ref. 24.
[c] See Ref. 25.
[d] The authors do not explicitly calculate this ratio nor do they give enough information for calculation of the error; however, we infer that the error in the ratio calculated from their figures and our M-intensity estimates (see Table I and Sec. III A) should be within the range 6 to 9%.
[e] See Ref. 26.
[f] This figure includes the data presented in Table IV, Ref. 19.

are given by the following expressions:

$$\sigma_c^2=(\epsilon^2/L^4\cos^4\lambda)A_N+KC_N/L\cos\lambda,$$

and

$$\sigma_\theta^2=(\epsilon^2/L^2\cos^2\lambda)B_N+KLE_N\cos\lambda,$$

with

$$K=(0.0187/\beta^2p^2)\ln(4.8p).$$

In each case, the first term is the contribution from measuring error, and the second term is the contribution from multiple scattering error. L is the track length in cm, ϵ is the point setting error in cm projected onto the fiducial plane, and A_N, B_N, C_N, and E_N are functions of the number of measured points N (evenly spaced along the track) as given in Ref. 34.

Although the resolution function is not Gaussian, we have used the conversion from rms to FWHM:

$$\Gamma=2.38\sigma_p/p,$$

appropriate for a Gaussian.

The seven measured resolution widths of Table II were fit to Eq. (5), varying the point setting error ϵ and the effective stereo angle θ_S. The best-fit values are $\epsilon=0.016$ cm and $\theta_S=26°$. The agreement between the seven measured points and Eq. (5) is shown in Table II. When applied to the μ^+-decay tracks, we obtain the FWHM as a function of momentum shown in Fig. 6.

IV. CORRECTIONS AND UNCERTAINTIES

A. Scanning Efficiency

In order to estimate the scanning efficiency, all of the film was scanned twice, and 20% of the sample-2 events were scanned four times. Suitable cutoffs in momentum, dip angle, and fiducial volume restricted the analysis to those events which unambiguously satisfied the selection criteria imposed during scanning. The usual method for estimating scanning efficiency, the method of Geiger and Werner,[35] was found to underestimate the number of events found on the third and fourth scans by a large factor. A more general method devised by Derenzo and Hildebrand[36] allows the events to fall into a visibility distribution and hence, takes into account the observed tendency of events missed by one scanner to be missed by other scanners.

The method of analysis may be briefly described as follows: The events are assumed to fall into a distribution $dN/dv=F(v)$, where dN is the number of events found by the average[37] scanner with probability between v and $v+dv$, and where v ranges from 0 to 1. The distribution of events found on the first average scan is thus $F(v)v$, leaving the distribution $F(v)(1-v)$ of unrecorded events. In general, the number of new events found on the ith average scan is given by the integral

$$M_i=\int_0^1 F(v)v(1-v)^{i-1}\,dv. \tag{6}$$

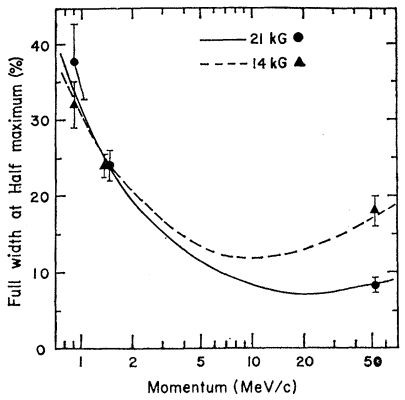

FIG. 6. Full width at half-maximum versus momentum. Curves show resolution as derived in Sec. III D for the 14- and 21-kG experiments. Points show measured values from Table II.

[35] H. Geiger and A. Werner, Z. Physik **21**, 187 (1924).

[36] S. E. Derenzo and R. H. Hildebrand, Nucl. Instr. Methods (to be published).

[37] The averaging method is described in Ref. 36.

TABLE IV. Inefficiencies.

Magnetic field	21 kG			14 kG		
Momentum range[a] (MeV/c)	0.5–2.5	2.5–4.5	4.5–6.5	0.5–2.5	2.5–4.5	4.5–6.5
Inefficiency (%) of first two scans predicted by Geiger-Werner method	6.3	2.0	1.4	17	3.1	1.5
New events recorded in third and fourth scans (% of total found in all four scans)	6.1	6.1	5.6	19	5.5	3.4
Lower limit (%) of inefficiency of first two scans[b]	7.1	6.5	6.3	23	5.9	4.9
Inefficiency (%) of first two scans predicted by method of Sec. IV A	8.4	6.7	7.0	27	6.4	4.8
Scanning inefficiency (%) used to correct sample 2[c]	7.2	5.5	5.9	24	5.3	4.1
Inefficiency (%) caused by annihilation in flight (see Sec. IV C)		0.3			0.4	
Inefficiency (%) due to fiducial volume (see Sec. IV C)		0.2			0.8	

[a] First bin extends below the region used in computing η.
[b] Derived by assuming $M_n/M_{n-1} \geq M_4/M_3$ for all $n>4$ (see Ref. 36).
[c] Taking into consideration the fact that some of the film was scanned four times.

The number of events undetected after four scans is

$$\sum_{i=5}^{\infty} M_i = \int_0^1 F(v)(1-v)^4\, dv.$$

As the pictures are of good quality with minimum-ionization tracks visible anywhere within the fiducial volume, an event will have low visibility only if it is hidden by its own unfavorable configuration or by superimposed tracks. Since it is unlikely that one track will exactly cover or smoothly join another, the distribution $F(v)$ should approach zero as v approaches zero.

A function that satisfies this condition and fits the data well is

$$F(v) = Av^{\alpha}(1-v)^{\beta}.$$

The parameters α and β were varied to minimize the χ^2 deviation between the observed M_i and the values given by Eq. (6). The results (see Table IV) were fit to a smooth function of momentum which was subsequently used to correct the observed spectra. We estimate the over-all uncertainty in the scanning efficiency to be 2%.

TABLE V. Summary of uncertainties in η ($\rho=\frac{3}{4}$).

	21-kG run	14-kG run	Combined[a]
Normalization from sample 1	0.10	0.09	0.06
Statistics of sample 2	0.13	0.12	0.09
Shape of resolution	0.13	0.08	0.08
Width of resolution	0.08	0.06	0.06
Momentum-scale distortions	0.11	0.10	0.09
Measuring efficiency	0.08	0.07	0.06
Scanning efficiency	0.11	0.10	0.09
	...	...	...
Combined in quadrature	0.28	0.24	0.20

[a] Uncertainties have been combined by estimating in each case the contributions from statistical and systematic (method-dependent) errors.

The correxponding uncertainties in η are shown in Table V.

B. Measuring Efficiency

Events that failed the first measurement were re-measured three times if necessary, but no attempt was made to measure those events which the scanners judged to be "unmeasurable" (0.28% of sample 1, 0.24% of sample 2, and 11.7% of conversion electrons). The over-all measuring efficiency was 97% for sample 1, 94% for sample 2, and 80% for conversion electrons.

It was necessary to estimate the momentum dependence of the measuring efficiency, since a large inefficiency at the low end of the 1–7 MeV/c interval would only slightly influence the over-all inefficiency. The method described in Ref. 19 was used with the 14-kG results shown in Fig. 7. Measuring efficiencies for the 21-kG

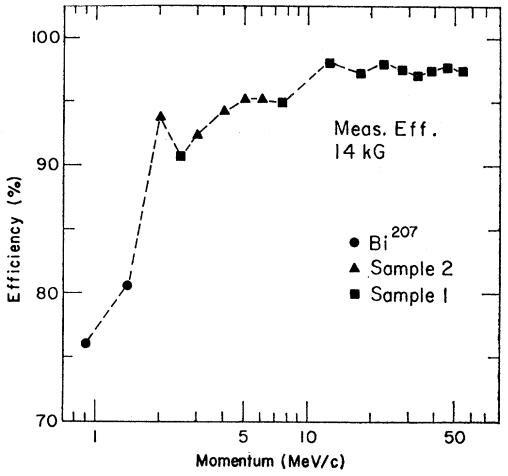

FIG. 7. Measuring efficiency for the 14-kG experiment. See Ref. 19 for method. Bi^{207} efficiencies based on 4923 events, sample-2 efficiencies based on 6820 events, and sample-1 efficiencies based on 11 280 events.

analysis (not shown) have been improved over those of Fig. 6, Ref. 19 and are close to the 14-kG values.

Unfortunately, the efficiencies determined from the Bi^{207} data are not directly applicable to μ-decay measurements, since the random timing of the conversion-electron emission with respect to the chamber expansion produces tracks of varying quality. Nevertheless, the measuring efficiencies of conversion electrons and positrons from μ^+ decay (see Fig. 7) are consistent with a single smooth curve (not shown). We estimate the over-all uncertainty in the measuring efficiency to be 1.5%. The corresponding uncertainties in η are shown in Table V.

C. Inefficiency Due to the $\frac{1}{4}$-Turn Requirement

The scanning requirement that the decay positron turn through more than 90° as seen in view one (as

discussed in Sec. II A) can eliminate valid events of momentum below 7 MeV/c if the positron annihilates in flight or leaves the sensitive volume of the chamber before making $\frac{1}{4}$ turn. The cross section for the annihilation in flight of positrons incident on stationary electrons[38] has been used to compute the probability of annihilation before $\frac{1}{4}$ turn.

Even though all events whose decay vertex was within 0.8 cm of the windows have been eliminated with the fiducial volume cut, there is a small probability that valid events of momentum below 7 MeV/c will leave the window before making $\frac{1}{4}$ turn. These inefficiencies are shown in Table IV for each magnetic field.

D. Shape and Width of the Resolution Function

The steepness of the μ^+-decay spectrum requires that the shape of the resolution function be well known, especially in the low-energy tail. As discussed in Sec. III A, analysis of the Bi^{207} data yields a plot of χ^2 as a function of the shape parameters a and b (see Fig. 5). When all corrections had been made, the fitted value of η (holding $\rho=\frac{3}{4}$) was tabulated as a function of a and b. The lines in Fig. 5 show values of a and b that yield equal values of η. The uncertainty in η due to the uncertainty in a and b, shown in Table V, has been estimated by combining the results of the Bi^{207} analysis (read directly from Fig. 5) with an allowance for the possible effects of differences in track quality between conversion electrons and μ^+-decay positrons. These errors were smaller for the 14-kG run, because this run had a resolution function whose tails were smaller and more accurately known.

To determine the uncertainty in the FWHM (see Fig. 6), Eq. (7) was multiplied by that factor which caused the fit to the data of Table II to become unsatisfactory. The uncertainty $\Delta\Gamma/\Gamma$ was 13% for the 21-kG run and 10% for the 14-kG run. The corresponding uncertainties in η are shown in Table V.

E. External Bremsstrahlung

It is possible for a high-energy positron to be included in sample 2 if it undergoes bremsstrahlung before making a track of sufficient length (approximately 1.5 cm) to be rejected by the scanners on the basis of curvature. The expected distribution must be corrected for this effect before it can be compared with the observed spectrum.

The probability that an electron of energy E_0 traversing 1.5 cm of liquid hydrogen will undergo bremsstrahlung and have a final energy in the interval between E_f and E_f+dE_f is given by the expression[39]

$$P(E_0,E_f)dE_f=\frac{6N_0\alpha}{A}\rho_H r_e\left[1+\left(\frac{E_f}{E_0}\right)^2-\frac{2}{3}\frac{E_f}{E_0}\right]\ln\left[\frac{2E_fE_0}{m_e(E_0-E_f)}\right]\frac{dE_f}{E_0-E_f}, \quad (7)$$

where α is the fine structure constant, N_0 is Avogadro's number, A is the atomic weight of hydrogen, r_e is the classical electron radius, m_e is the electron mass, and ρ_H is the density of the hydrogen. The change in the spectrum is given by

$$\Delta N(E;\rho,\eta)=\int_{E_f+E_{\gamma\min}}^{\frac{1}{2}m_\mu} N(E';\rho,\eta)P(E',E)dE' - \int_0^{E_f-E_{\gamma\min}} N(E;\rho,\eta)P(E,E')dE', \quad (8)$$

where m_μ is the muon mass and $E_{\gamma\min}$ is a lower cutoff in γ-ray energy. The first integral gives the contributions from higher energies and the second gives the contributions to lower energies. Equation (7) is valid when the initial, final, and γ-ray energies are highly relativistic, necessitating the cutoff $E_{\gamma\min}$. Equation (8) was found to be insensitive to the value of this cutoff in the range from 0.5 to 2 MeV.

Equation (8) (with $E_{\gamma\min}=0.5$ MeV) was used to correct the expected distributions as discussed in Sec. V. The magnitude of this correction is equivalent to a shift of 0.08 in η.

F. Momentum-Scale Distortions

1. Magnetic-Field Variations

The variations in the magnetic field were less than 1% over the visible region of the chamber. As the average value of the magnetic field was used during the 21-kG track reconstruction, only a nonuniform track distribution could bias the momentum scale. Systematic momentum error from this source was below 0.2%. The 14-kG analysis used a linear combination of solutions of Maxwell's equations which had been fit to a measured field map, and for this run, the systematic momentum error due to magnetic-field variations was below 0.1%.

2. Uncertainty in the Stopping Power of Liquid Hydrogen

The track-fitting program determined the momentum at the center of the track and used a range-momentum table to compute the momentum at the point of origin. The tables of energy losses of e^- and e^+ by Berger and Seltzer[21] were modified to construct tables specifically for this experiment by excluding collision losses greater

[38] A. I. Akhiezer and V. B. Berestetskii, *Quantum Electrodynamics* (Technical Information Service, Oak Ridge, Tenn., 1957).

[39] H. W. Koch and J. W. Motz, Rev. Mod. Phys. **31**, 920 (1959).

than 0.35 MeV/c. Since the implementation of this cutoff on the scanning table was subject to variations in interpretation (the scanners were instructed to measure the momentum of only those δ rays that made more than $\frac{1}{4}$ turn), a 2% uncertainty in the rate of energy loss was introduced. The conversion electrons were reconstructed using the modified electron table, and the positrons from μ^+ decay were reconstructed using the modified positron table.

The density of hydrogen used in this experiment was determined by measuring the length of μ^+ from π^+ decay. Measuring error was negligible (0.5%), and straggling error was 3.5%. The μ^+ tracks were chosen to have low dip and a configuration which permitted the highest precision in placing the crosshair upon the $\pi^+-\mu^+$ and μ^+-e^+ track intersection points. The Bethe stopping-power formula[40] was used to determine the density from the measured μ^+-track length (and known energy) using an average ionization potential of 18.7 eV.[21] The density was found to vary between 0.0549 $\pm$0.0005 and 0.0566$\pm$0.0004 g/cm^3 during the runs. Each section of film was analyzed using the appropriate density.

We estimate the over-all uncertainty in energy loss to be 3%. On the average, conversion electrons and sample-2 positrons suffer a 10% momentum correction when their momentum is converted from the center of the track to the point of origin. A 3% error in stopping power would shift their momentum by 0.3%. Sample-1 positrons suffer a 5% correction. A 3% error in stopping power would shift their momentum by 0.15%.

3. *Effect of Systematic Momentum Shift on Determination of* η

The detailed mechanism of momentum error is sufficiently complicated so that it is not *a priori* obvious what parameter to use for the "position" of a line. The results of our calibration indicate that the parameter p' in Eq. (3) is 0.5$\pm$0.7% below the true line position for $a=0.4$, $b=2.8$, and 1.5$\pm$0.6% below the true line position for $a=1.2$, $b=3.2$.

The corresponding uncertainties in η are shown in Table V.

G. Statistics of Samples 1 and 2

The uncertainty in determining the total number of decays scanned using sample 1 (which is 1% of all decays) is almost completely statistical, as nonstatistical fluctuations in beam intensity were at a level too small to be observed. The uncertainty in η due to the limited statistics of sample 2 was determined in the usual manner by observing the change in η required to increase the χ^2 of the fit by one unit. See Table V for these uncertainties in η.

[40] H. A. Bethe, Ann. Physik **5**, 325 (1930); Z. Physik **76**, 293 (1932); B. Rossi, *High-Energy Particles* (Prentice-Hall, Inc., Englewood Cliffs, N. J., 1965), p. 24, Eq. (7).

V. ANALYSIS OF SAMPLES 1 AND 2

The measuring efficiency as a function of momentum (shown in Fig. 7) was determined for samples 1 and 2 using the method described in Ref. 19. The scanning efficiency as a function of momentum was estimated using the analysis of Sec. IV A and Ref. 36. After making fiducial volume and dip selections, we corrected the observed spectra for all inefficiencies and for the systematic momentum shift discussed in Sec. III D. The resulting distributions are shown in Table VI and in Figs. 8 and 9.

The muon-decay spectrum of Michel [Eq. (2)] was modified by the internal electromagnetic correction[14–16] and by correction for external bremsstrahlung (see Sec. IV E). Our known momentum-dependent resolution function [Eqs. (3) and (5)] was then folded into the result. The calculated distributions were tabulated on a grid of η and ρ to be compared directly with the measured spectra.

Two ways of making this comparison are described as follows:

(i) Comparison of sample 1 with an expected distribution having the same number of events in the interval from 2.6 to 47 MeV/c.

TABLE VI. Measured low-momentum spectrum: (A) 21 kG. (B) 14 kG.

(A) 21-kG distribution of events in sample 2 found among 607 000 decays of all momenta.

Momentum interval[a]	n_0=events observed	n_e=corrected number of events[b]	n_n=events per 10^6 decays[c]	Events expected per 10^6 decays[d] $\eta=0$, $\rho=\frac{3}{4}$
0.03–0.04	61	74	122	168
0.04–0.05	96	114	188	229
0.05–0.06	149	175	300	299
0.06–0.07	175	204	343	379
0.07–0.08	226	263	433	469
0.08–0.09	274	318	516	568
0.09–0.10	346	400	659	677
0.10–0.11	438	506	833	796
0.11–0.12	485	559	921	924
0.12–0.13	529	609	1003	1061
	...	...	...	...
0.03–0.13	2779	3222	5318	5570

(B) 14-kG distribution of events in sample 2 found among 739 000 decays of all momenta.

0.03–0.04	90	118	160	158
0.04–0.05	133	165	223	218
0.05–0.06	186	223	302	287
0.06–0.07	258	301	407	366
0.07–0.08	283	324	439	455
0.08–0.09	357	402	544	553
0.09–0.10	445	496	671	661
0.10–0.11	542	598	809	779
0.11–0.12	594	650	880	906
0.12–0.13	679	738	999	1042
	...	...	...	...
0.03–0.13	3567	4015	5434	5425

[a] Momentum, in units of $p_{max}=\frac{1}{2}m_\mu c$.
[b] Corrected for the inefficiencies of Sec. IV A–Sec. IV C.
[c] $n_n=10^6 n_e/7.39\times10^5$.
[d] Assuming the Michel theory [Eq. (2)], $\rho=\frac{3}{4}$, resolution as given by Eqs. (3) and (5), and radiative corrections as given in Ref. 16.

(ii) Comparison of sample 2 with an expected distribution having a total of $N_1(F_2/F_1)$ events, where N_1 is the number of events in sample 1 and (F_2/F_1) is the ratio of the number of frames scanned for sample-2 events to the number of frames scanned for sample-1 events. This ratio is close to 99.

VI. RESULTS

A. Determination of η and ρ

Table VII presents a summary of the fitting of the measured spectrum to the expected distributions. It is

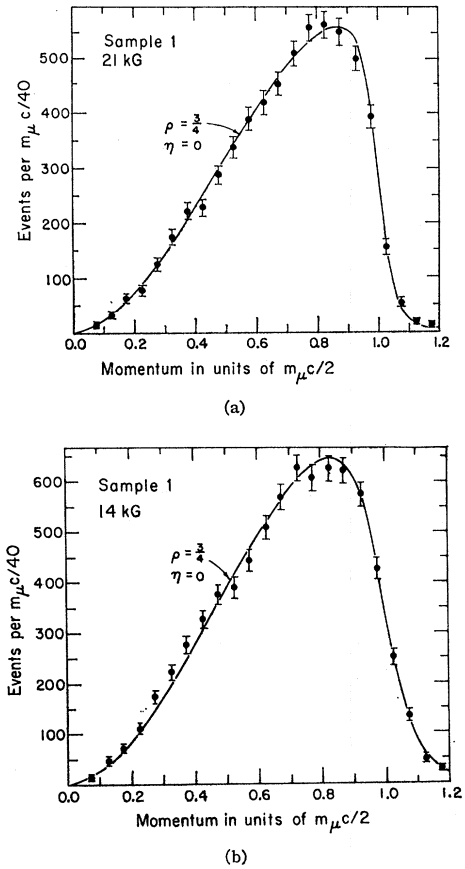

FIG. 8. Muon-decay spectra. Data from sample 1 for 21 kG (6123 events) and 14 kG (7469 events) corrected for scanning and measuring efficiencies. Curves show $\rho=\frac{3}{4}$, $\eta=0$ spectrum.

seen that the sample-1 spectrum is in good agreement with the $V-A$ theory and with previous work.[3–7]

Constraining ρ to be $\frac{3}{4}$ and using the radiative corrections of Grotch,[16] the 21-kG run yields $\eta=-0.40\pm0.28$ and the 14-kG run yields $\eta=+0.05\pm0.24$. The weighted average of these two figures is $\eta=-0.13\pm0.20$. The radiative corrections of Refs. 1, 14, and 15 result in values for η which differ by less than 0.01 from those presented here. Statistical errors have been added in quadrature, and systematic errors have been averaged (see Table V for errors in η).

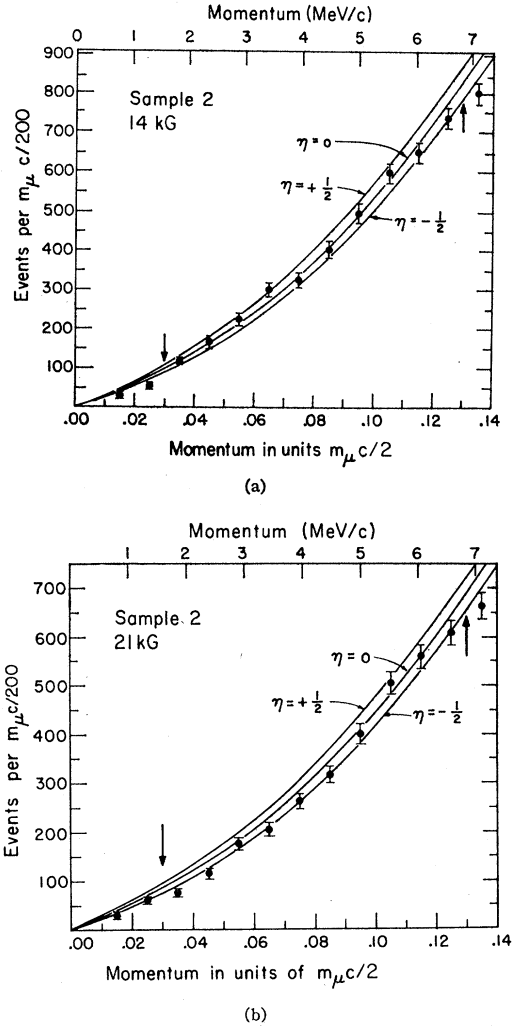

FIG. 9. Low end of spectrum. Points show distribution of events below 7.4 MeV/c for 21 kG (3975 events) and 14 kG (4853 events) corrected for scanning and measuring efficiencies. Curves show spectra calculated for $\eta=0$ and $\eta=+0.5$ assuming $\rho=\frac{3}{4}$, radiative corrections as in Ref. 16, and spectrometer resolution as given by Eqs. (3) and (5). Arrows show limits of momentum range used in this analysis. See Tables VI and VII for data and results of fits.

A two-parameter fit incorporating published data from spark-chamber measurements[5–7] of the upper half of the spectrum gives the values $\eta=-0.12\pm0.21$ and $\rho=0.752\pm0.003$.

B. Tests for Systematic Error

In order to check for biases in the experiment, the following procedures were carried out:

(i) The upper and lower momentum cutoffs of sample 2 were varied. A decrease in the upper cutoff from 6.8 to 6.3 MeV/c changed the fitted value of η by less than 0.05. An increase in this cutoff to 7.9 MeV/c lowered the fitted value of η by 0.22 due to the loss of events with

TABLE VII. Measured values for η and ρ.

Sample[a] (or experimenter)	Field (kG)	Momentum range (units: $\frac{1}{2}m_\mu c$)	η	ρ	Remarks
1	21	0.05–0.90	$\equiv 0$	0.760 ± 0.037	Fit: $\chi^2=14.4$: 16 deg freedom
	14	0.05–0.90	$\equiv 0$	0.694 ± 0.037	Fit: $\chi^2=12.8$: 16 deg freedom
2	21	0.03–0.13	-0.32 ± 0.29[b]	$\equiv\frac{3}{4}$	Fit: $\chi^2=8.5$; 9 deg freedom
	21	0.03–0.13	-0.40 ± 0.28[c]	$\equiv\frac{3}{4}$	$\chi^2=12.2$; 9 deg freedom
	14	0.03–0.13	$+0.05\pm0.24$	$\equiv\frac{3}{4}$	$\chi^2=7.6$; 9 deg freedom
	14+21	0.03–0.13	-0.13 ± 0.20	$\equiv\frac{3}{4}$	Average of previous 2 results
Plano[d]		Whole spectrum	(-2.0 ± 0.9)	0.745 ± 0.025	Author discounts value for η
Peoples[e]		>0.4	$+0.05\pm0.5$	$\equiv\frac{3}{4}$	$\eta=0$ yields $\rho=0.7503\pm0.0026$
Sherwood[f]		>0.5	$-0.7\ \pm0.6$	$\equiv\frac{3}{4}$	$\eta=0$ yields $\rho=0.760\pm0.009$
Fryberger[g]		>0.45	$-0.7\ \pm0.5$	$\equiv\frac{3}{4}$	$\eta=0$ yields $\rho=0.762\pm0.008$
Refs. 5–7 combined		>0.4	$\lvert\eta\rvert<0.5$	0.752 ± 0.005	Error on ρ corresponding to *assumed* limits on η
Sample 2 and Refs. 5–7		0.03–0.13 >0.4	-0.12 ± 0.21	0.752 ± 0.003	See Fig. 10

[a] Sample 1: events from every hundredth frame. Sample 2: events of projected momentum <7.1 MeV/c from all other frames.
[b] As in S. E. Derenzo and R. H. Hildebrand, Phys. Rev. Letters **20**, 614 (1960).
[c] Previous result with improved energy-loss tables (Ref. 21), improved resolution function (described in Sec. III), and external bremsstrahlung corrections (described in Sec. IV E).
[d] See Ref. 4. [e] See Ref. 5. [f] See Ref. 6. [g] See Ref. 7.

projected momentum greater than 7.1 MeV/c. Variations of 0.10 in the fitted value of η were observed as the lower cutoff was decreased from 1.6 to 0.5 MeV/c.

(ii) As Eq. (2) is valid only for unpolarized muons, an error would be expected if muons emitted along the field were detected with different efficiency than those emitted against the field. When muons of low dip angle were selected (i.e., muons depolarized by precession in the magnetic field), and when electrons of low dip angle were selected (which carry the least amount of asymmetry information), no significant change in the fitted value of η occurred (see Table I of Ref. 11).

(iii) The fiducial volume was reduced by 13% without a significant change (less than 0.05) in the fitted value of η.

VII. CONCLUSIONS

This work, the first measurement of the low-momentum end of the μ^+-decay spectrum, complements the results of previous experiments[5–7] in the higher-momentum range where the correlation between η and ρ is such that η can be derived only by assuming a precise value (e.g., $\frac{3}{4}$) for ρ, and ρ can be derived only by assuming a precise value (e.g., zero) or a range of possible values (e.g., $-\frac{1}{2}$ to $+\frac{1}{2}$) for η. By contrast, when the η-ρ correlation from this experiment is combined with the correlation from the 26–53 MeV data, then η and ρ are completely uncorrelated (see Fig. 10).

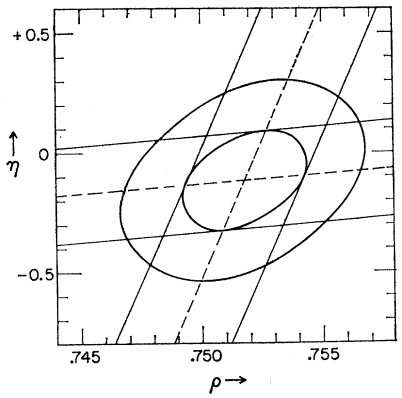

FIG. 10. ρ-η correlation. The nearly vertical lines show the correlation from the higher-momentum measurements of Refs. 5–7, where the slopes and intercepts are weighted averages (slope for Ref. 5 inferred from uncertainties given for ρ and η). The lines of lower slope show the correlation from this experiment. The ovals are one- and two-standard-deviation contours which result when the data of this and the previous experiments are combined.

In the following subsections, the experimental results are interpreted in terms of the weak-interaction coupling constants, the electromagnetic correction, and the mass of the intermediate vector boson.

A. Experimental Limits on the Coupling Constants

As shown in the Appendix, the most recent values of the five decay parameters restrict the coupling constants as follows:

$$g_S \lesssim 0.33 g_V, \qquad g_P \lesssim 0.33 g_V,$$
$$0.76 g_V \lesssim g_A \lesssim 1.20 g_V, \quad \phi_{AV} = 180° \pm 15°,$$
$$g_T \lesssim 0.28 g_V,$$

in the most general local, lepton-conserving interaction (see Appendix for definitions).

Since the radiative corrections are unambiguous only for the case of vector and axial-vector coupling, it is more consistent (although less general) to set $g_S = g_P = g_T = 0$ and solve for g_A and the phase angle ϕ_{AV}. The results follow:

$$0.75 g_V \lesssim g_A \lesssim 1.20 g_V \quad \text{and} \quad \phi_{AV} = 180° \pm 16°.$$

Within the framework of the two-component neutrino theory only vector-type interactions remain, and the following relations hold among them: $C_A' = -C_A$ and $C_V' = -C_V$. In the complex plane, ϕ_{AV} is the phase angle between C_A and C_V and the amplitude of violation of time-reversal invariance is restricted as

$$\sin\phi_{AV} = 0.0 \pm 0.27.$$

B. Tests of the Electromagnetic Correction to the Muon-Decay Spectrum

It is possible to interpret measurements of the muon-decay spectrum as a test of the electromagnetic correction, under the assumptions that the interaction is local and that $\rho=\frac{3}{4}$ and $\eta=0$. To do this, the spectrum is parametrized in terms of a quantity C rather than in terms of ρ and η. C is defined to be 0 for the uncorrected Michel spectrum and 1 for the corrected spectrum, linear interpolation being used for intermediate values.

The data of sample 2 can be described by the curve $\eta=-0.13\pm0.20$, $\rho=\frac{3}{4}$, and $C=1$. This is equivalent to $\eta=0$, $\rho=\frac{3}{4}$, and $C=0.91\pm0.13$.

Similarly, the data from Refs. 5–7 may be described by the curve $\eta=0$, $\rho=0.7523\pm0.0024$, and $C=1$, which is equivalent to $\eta=0$, $\rho=\frac{3}{4}$, and $C=0.959\pm0.043$.

C. Vector Boson

If the decay of the muon is mediated by a vector boson, both the isotropic spectrum and the radiative corrections to it must be altered. Assuming a nonlocal $V-A$ theory, Bailin[18] has derived an expression for the altered spectrum in terms of the vector-boson mass. As in the case of the local $V-A$ theory, the radiative corrections are finite, the virtual photon divergence canceling with the real photon divergence.

A 1-GeV vector boson would alter the fitted value of ρ by 0.0034 through its modification of the purely weak interaction and by 0.0001 through its modification of the radiative correction. The experimental high-momentum spectrum[5–7] is fitted by the curve $\rho=0.7523\pm0.0024$, $\eta=0$, and if the deviation of ρ from $\frac{3}{4}$ is interpreted as due to the effects of a vector boson, we obtain

$$(m_\mu/m_W)^2=0.0066\pm0.0069,$$
$$m_W=1.3^{+\infty}_{-0.4}\ \text{GeV}.$$

Thus, the one-standard-deviation lower bound on the mass of the vector boson m_W is 0.9 GeV.

The low-momentum spectrum is also sensitive to the mass of the vector boson, being depleted by 2% for a mass of 1 GeV. Our measurement of the low-momentum spectrum sets a one-standard-deviation lower bound of 0.3 GeV on the vector-boson mass.

ACKNOWLEDGMENTS

I wish to thank Professor R. H. Hildebrand for suggesting this experiment and for his advice and generous assistance through its difficult problems. I also wish to thank my colleagues R. Klem, J. Klems, C. Rose, and C. Vossler for assistance during the chamber operation. I am indebted to S. Lucero for his skillful mechanical design and development work in connection with the Bi^{207} source and bubble chamber. I am also indebted to M. S. Freedman, F. T. Porter, and F. Wagner for recommending Bi^{207} as a suitable conversion-electron source, for giving advice on techniques for its use, and for providing a sample. I am grateful to S. Berman, G. Conforto, D. Fryberger, B. Sherwood, V. Telegdi, and R. Winston for interesting and stimulating discussions. I wish to give thanks to F. T. Solomitz for advice on the use of the Three-View Geometry Program; to F. P. Brady and R. A. Warner for a communication concerning conversion-electron intensities; and to M. J. Berger and R. L. Platzman for supplying tables of stopping power for electrons and positrons in liquid hydrogen. I wish to acknowledge with thanks, support from an AMU-ANL predoctoral fellowship and a Shell Foundation fellowship during part of this work. Finally, I wish to thank the scanners and measurers, too numerous to list here, who painstakingly scanned and measured over 18 miles of bubble-chamber film.

APPENDIX: EXPERIMENTAL LIMITATIONS OF THE COUPLING CONSTANTS

In terms of the charge-retention Hamiltonian [Eq. (1)], the five decay parameters related to the spectrum (ρ,η), asymmetry (ξ,δ), and helicity (h) of the decay electrons are given by the following expressions[41]:

$$\rho=[3g_A^2+3g_V^2+6g_T^2]/D,$$
$$\eta=[g_S^2-g_P^2+2g_A^2-2g_V^2]/D,$$
$$\xi=[-6g_Sg_P\cos\phi_{SP}+8g_Ag_V\cos\phi_{AV}-14g_T^2\cos\phi_{TT}]/D,$$
$$\delta=[6g_Ag_V\cos\phi_{AV}-6g_T^2\cos\phi_{TT}]/D\xi,$$
$$h=[2g_Sg_P\cos\phi_{SP}-8g_Ag_V\cos\phi_{AV}-6g_T^2\cos\phi_{TT}]/\mathrm{D},$$

where

$$D=g_S^2+g_P^2+4g_A^2+4g_V^2+6g_T^2,$$
$$g_i^2=|C_i|^2+|C_i'|^2,$$

and

$$\cos\phi_{ij}=-\mathrm{Re}(C_i^*C_j'+C_i'C_j^*)/g_ig_j.$$

The quantities g_i are defined to be real positive numbers, and the ϕ_{ij} are phase angles between the i-type and j-type interactions. Under the assumption that $C_i'=-C_i$ and $C_j'=-C_j$ (two component neutrinos), then S, P, and T terms vanish, and ϕ_{AV} is the phase angle between C_A and C_V in the complex plane.

Because of the structure of these equations, it is possible for five decay parameters to place limits on the following seven quantities:

$$g_S/g_V,\ g_P/g_V,\ g_A/g_V,\ g_T/g_V,\ \phi_{SP},\ \phi_{AV},\ \text{and}\ \phi_{TT}. \quad (9)$$

Those related to the polarization of the neutrinos (such as C_i/C_i') will remain unmeasurable until the neutrinos can be studied directly.

We now wish to determine the allowable limits on these seven quantities as restricted by the experimental values and errors of the five decay parameters. To do this, we define a χ^2 that indicates how significantly ρ,

[41] We have used the definitions and sign conventions of T. Kinoshita and A. Sirlin, Phys. Rev. **108**, 844 (1957).

TABLE VIII. Experimental limitations on the coupling constants.[a]

Decay parameter	$V-A$	1964[b]	1967[c]	1968[d]
ρ	$\frac{3}{4}$	0.078 ± 0.025	0.7523 ± 0.0046	0.7518 ± 0.0026
η	0	···	$-\frac{1}{2}\leqslant\eta\leqslant+\frac{1}{2}$	$-0.12\ \pm0.21$
ξ	-1	$-0.94\ \pm0.07$	$-0.973\ \pm0.014$	$-0.973\ \pm0.014$
δ	$\frac{3}{4}$	$0.78\ \pm0.05$	0.7540 ± 0.0085	0.7540 ± 0.0085
h	1	$1.04\ \pm0.18$	$1.00\ \pm0.13$	$1.00\ \pm0.13$
Coupling constant[a]				
g_S, g_P	0	$\leqslant0.38$	$\leqslant0.36$	$\leqslant0.33$
g_A	1	$0.69\leqslant g_A\leqslant1.44$	$0.76\leqslant g_A\leqslant1.32$	$0.76\leqslant g_A\leqslant1.20$
ϕ_{AV}	180°	$180°\pm21°$	$180°\pm16°$	$180°\pm15°$
g_T	0	$\leqslant0.45$	$\leqslant0.30$	$\leqslant0.28$

[a] In units of g_V.
[b] This column uses the experimental values of the decay parameters which were available when Ref. 42 was written.
[c] This column uses the values of the decay parameters known before our low-energy measurement.
[d] This column incorporates our low-energy measurement.

η, ξ, δ, and h deviate from their experimental values ρ_0, η_0, ξ_0, δ_0, and h_0 in units of their experimental uncertainties σ_ρ, σ_η, σ_ξ, σ_δ, and σ_h;

$$\chi^2=(\rho-\rho_0)^2/\sigma_\rho^2+(\eta-\eta_0)^2/\sigma_\eta^2+(\xi-\xi_0)^2/\sigma_\xi^2+(\delta-\delta_0)^2/\sigma_\delta^2+(h-h_0)^2/\sigma_h^2. \quad (10)$$

Unlike previous work done along these lines,[7,42] this analysis makes no approximations in relating uncertainties in the five decay parameters to uncertainties in the seven quantities (9), and allows for the fact that the experimental values of the decay parameters differ from the $V-A$ values.

As a first step, the seven quantities were varied to minimize the χ^2 in Eq. (10). This minimum will be designated χ_0^2. The statistically allowable range of each of the quantities was then determined as its smallest and largest value within the χ_0^2+1 hypersurface. This procedure takes into consideration any correlations with the other six quantities. The results are shown in Table VIII. As g_S, g_P, and g_T are consistant with zero, no limits may be placed on the phase angles ϕ_{SP} and ϕ_{TT}.

When the coupling constants are set to their $V-A$ values, the most recent values of the decay parameters yield $\chi^2=4.7$ for 5 deg of freedom. Thus, the experimental measurements are in good agreement with the $V-A$ theory.

[42] C. Jarlskog, Nucl. Phys. **75**, 659 (1966).

PHYSICAL REVIEW VOLUME 181, NUMBER 5 25 MAY 1969

Cabibbo Theory, Pole Dominance, and Sum Rules for Radiative Decays of Pseudoscalar Mesons*

GERALD W. INTEMANN
Department of Physics, State University of New York, Binghamton, New York 13901
(Received 9 December 1968)

By extending the Cabibbo theory to the radiative leptonic decay $\pi^+\to\pi^0+l^++\nu_l+\gamma$, we analyze the vector and axial-vector form factors which describe this decay. Assuming unsubtracted dispersion relations for these form factors at *fixed* momentum transfer as well as pole dominance, we obtain a number of sum rules relating the masses and couplings of the ω, ρ, A_1, and A_2 mesons. In addition, we obtain, using current algebra and the hypothesis of a partially conserved axial-vector current, a soft-pion theorem relating the vector form factors of the decay $\pi^+\to\pi^0+l^++\nu_l+\gamma$ to the axial-vector form factor associated with $\pi^+\to l^++\nu_l+\gamma$. For those sum rules that can be tested, excellent agreement is obtained with the experimental data. A similar analysis is made of the decay $K^+\to\pi^0+l^++\nu_l+\gamma$, and a corresponding set of sum rules is obtained relating the masses and couplings of the ω, K^*, K_V, and K_A mesons.

I. INTRODUCTION

FOR some time now, there has been a great deal of interest in the radiative decays of the pseudoscalar mesons.[1–6] Using the algebra of currents and the assumption of unsubtracted dispersion relations, a number of authors[1–5] have obtained sum rules which seem to be well satisfied experimentally. Recently, the radiative decays $\pi^+\to l^++\nu_l+\gamma$ and $K^+\to l^++\nu_l+\gamma$ have also been examined from the viewpoint of the Cabibbo theory.[6] This work has led to information about the vector and axial-vector form factors describing these decays which seems to agree with the limited experimental data.[7]

In this paper we extend the results of Ref. 6 by studying the radiative decays $\pi^+\to\pi^0+l^++\nu_l+\gamma$ and $K^+\to\pi^0+l^++\nu_l+\gamma$. We examine both the vector and

* Work supported in part by the Research Foundation of the State University of New York under Fund No. 040-7113-A.
[1] Fayyazuddin and Riazuddin, Phys. Rev. Letters **18**, 715 (1967).
[2] J. S. Vaishya and K. C. Gupta, Phys. Rev. **165**, 1696 (1968).
[3] S. G. Brown and G. B. West, Phys. Rev. **168**, 1605 (1968).
[4] Riazuddin and Fayyazuddin, Phys. Rev. **171**, 1428 (1968).
[5] C. S. Lai, Nucl. Phys. **B9**, 521, (1969).
[6] P. De Baenst and J. Pestieau, Nuovo Cimento **53A**, 407 (1968).
[7] Indeed, there appear to be only two sets of experimental data on $\pi^+\to l^++\nu_l+\gamma$. See P. Depommier *et al.*, Phys. Letters **7**, 285 (1963); Booth *et al.*, Proc. Phys. Soc. (London) **86**, 1317 (1965).

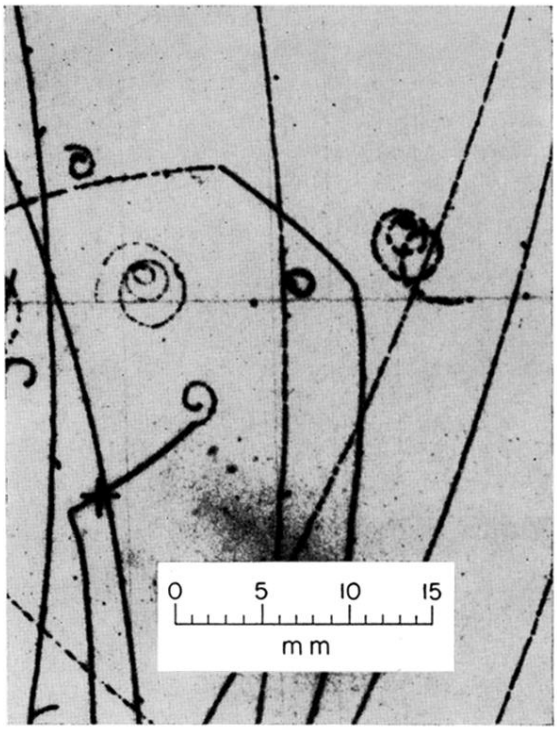

FIG. 3. Sample events. Picture shows two 1.4-MeV/c internal-conversion electrons emerging from the Mylar strip (faint horizontal line), and two $\pi^+ - \mu^+ - e^+$ decay chains. One of the positrons has a momentum of 0.7 MeV/c.